Mononuclear Mn Complexes Featuring N, S-/N, N-donor and 1,3,5-triaza-7-phosphaadamantane ligands: Synthesis and Electrocatalytic Properties

Vishakha Kaim and Sandeep Kaur-Ghumaan*

Department of Chemistry, University of Delhi, Delhi 110007, India

Email: skaur@chemistry.du.ac.in

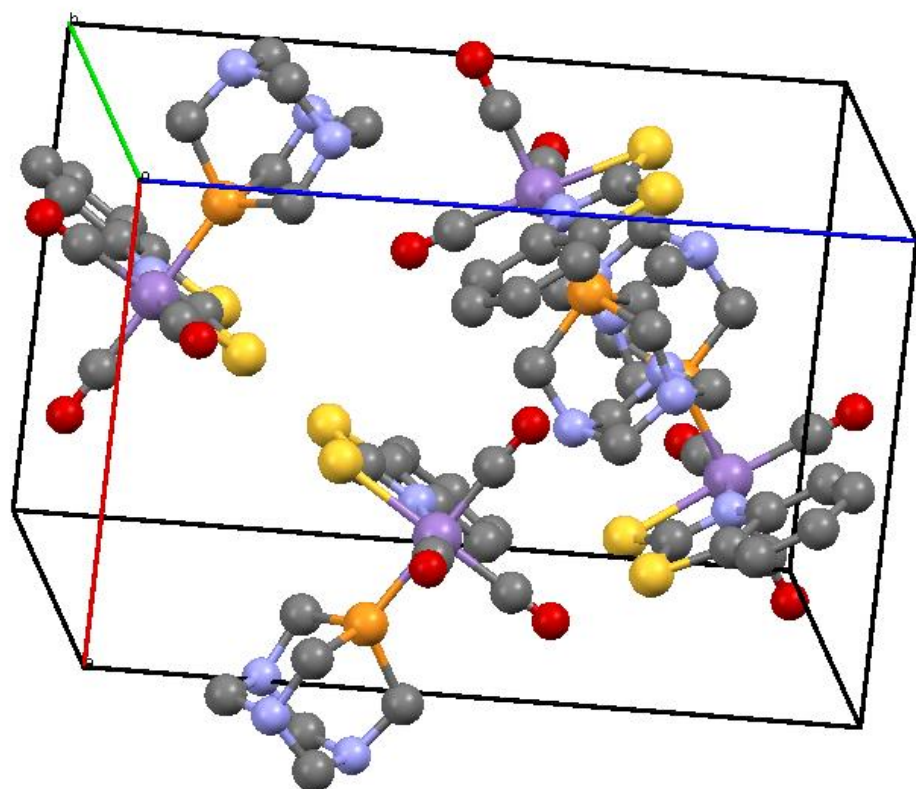**Electronic Supplementary Information**

New Journal of Chemistry

Figure S1. Crystal packing of complex **1** along the *b* axis.
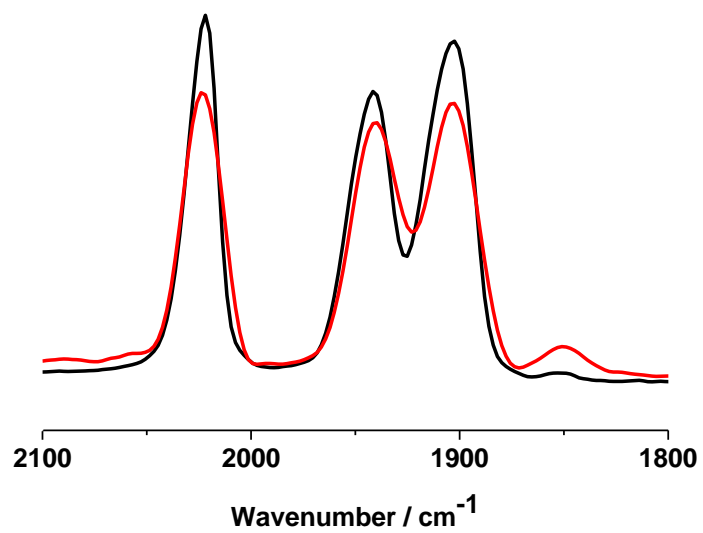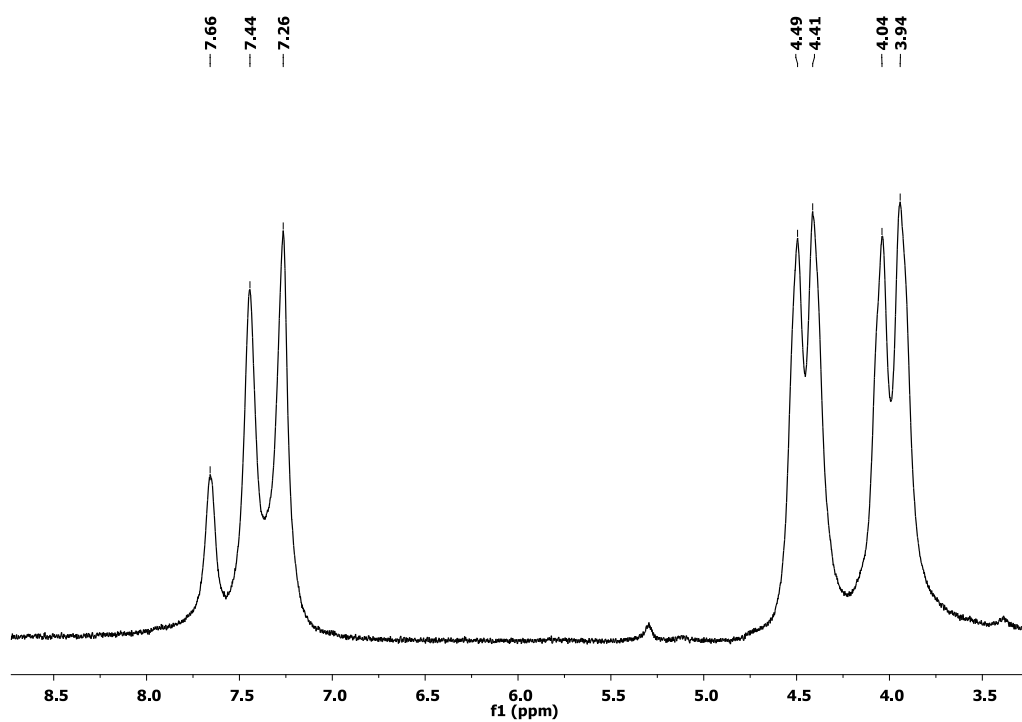
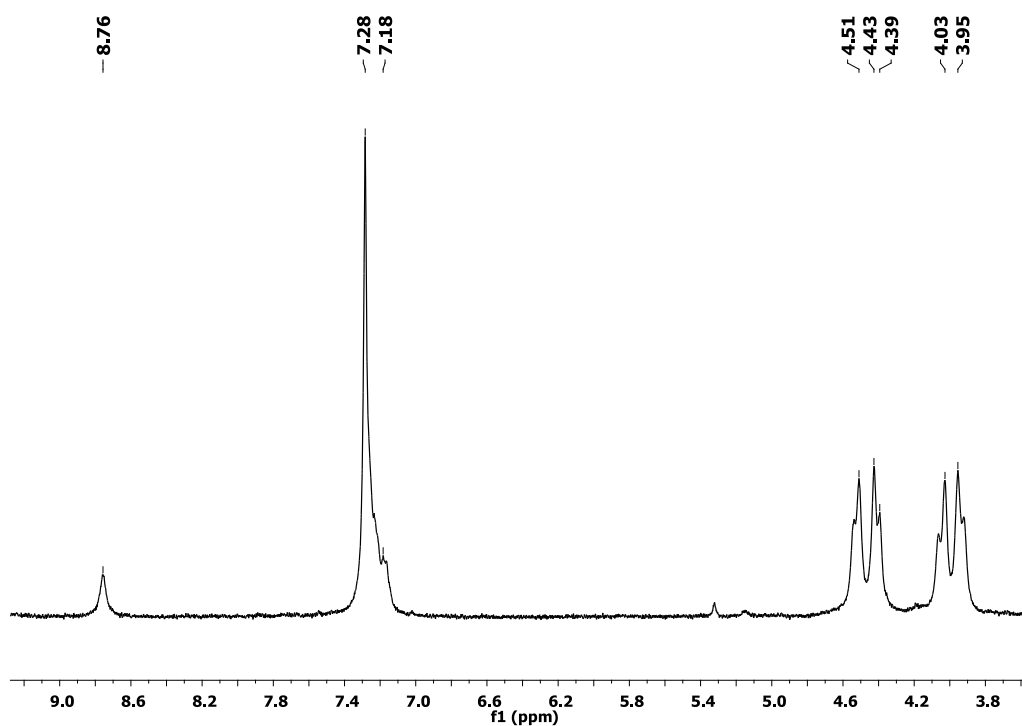**Figure S2.** FTIR spectra for complexes **1** (—) and **2** (—) in dichloromethane.

a)

b)

Figure S3. ^{1}H NMR spectra for complexes (a) **1** and (b) **2** (400 MHz, CDCl$_3$, 298 K).

(a)

--28.96

400 350 300 250 200 150 100 50 0 -50   -150   -250   -350

δ / ppm

(b)

--29.17

400 350 300 250 200 150 100 50 0 -50 -100 -150 -200 -250 -300 -350 -400
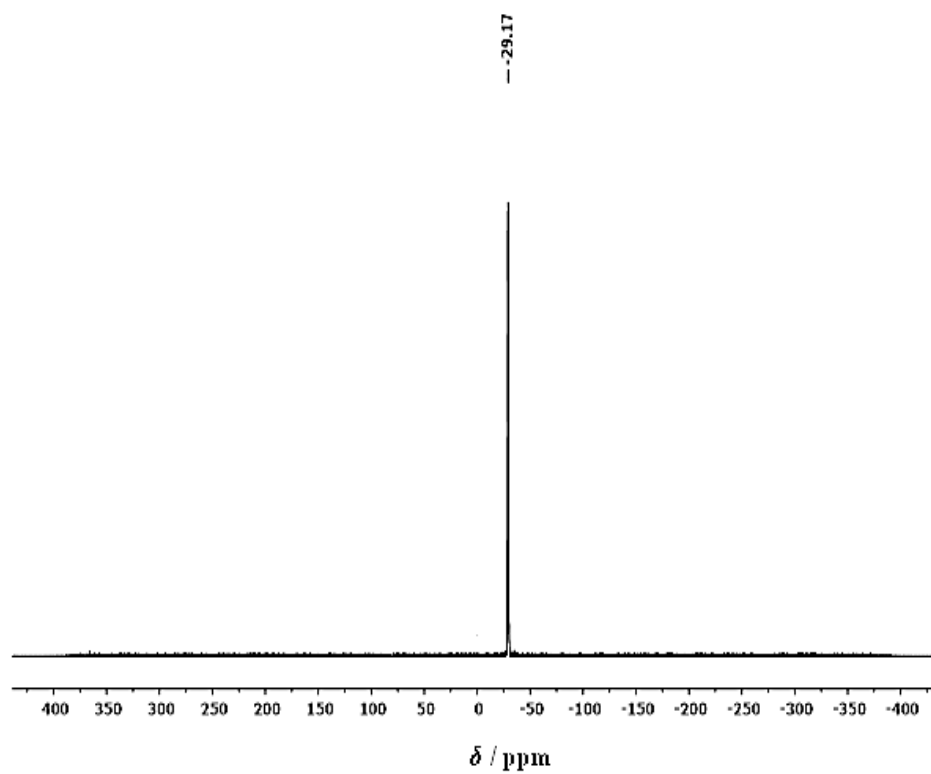
δ / ppm
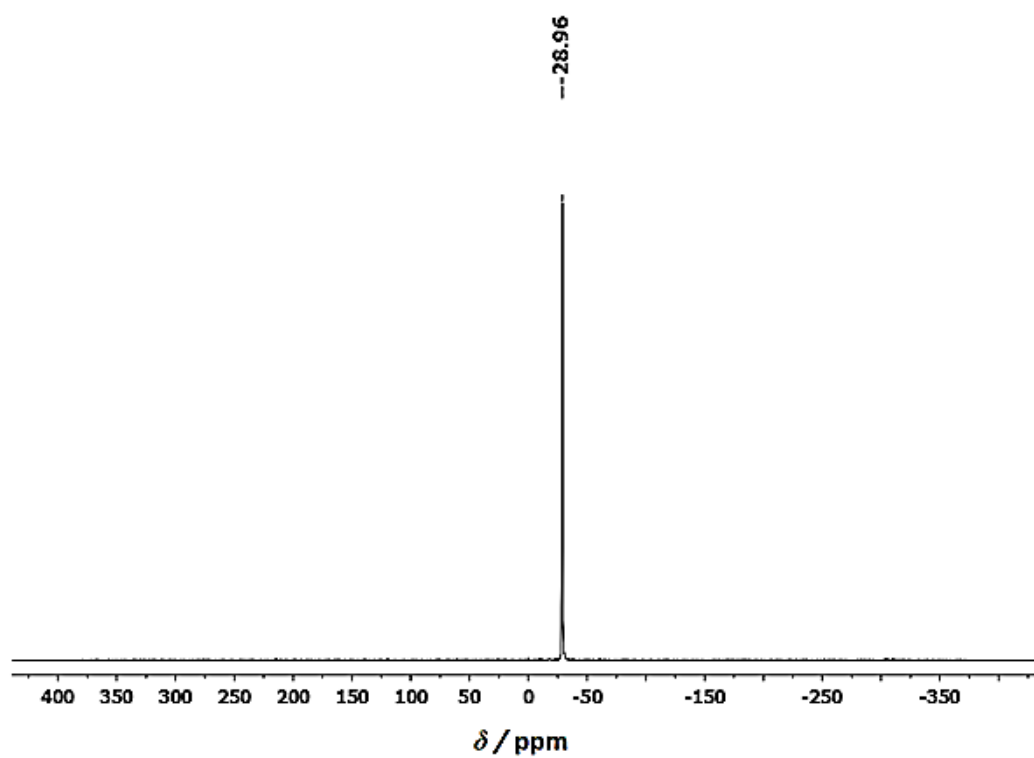
Figure S4. ^{31}P {^{1}H} NMR spectra for complexes (a) **1** and (b) **2** (161.8 MHz, CDCl$_3$, 298 K).
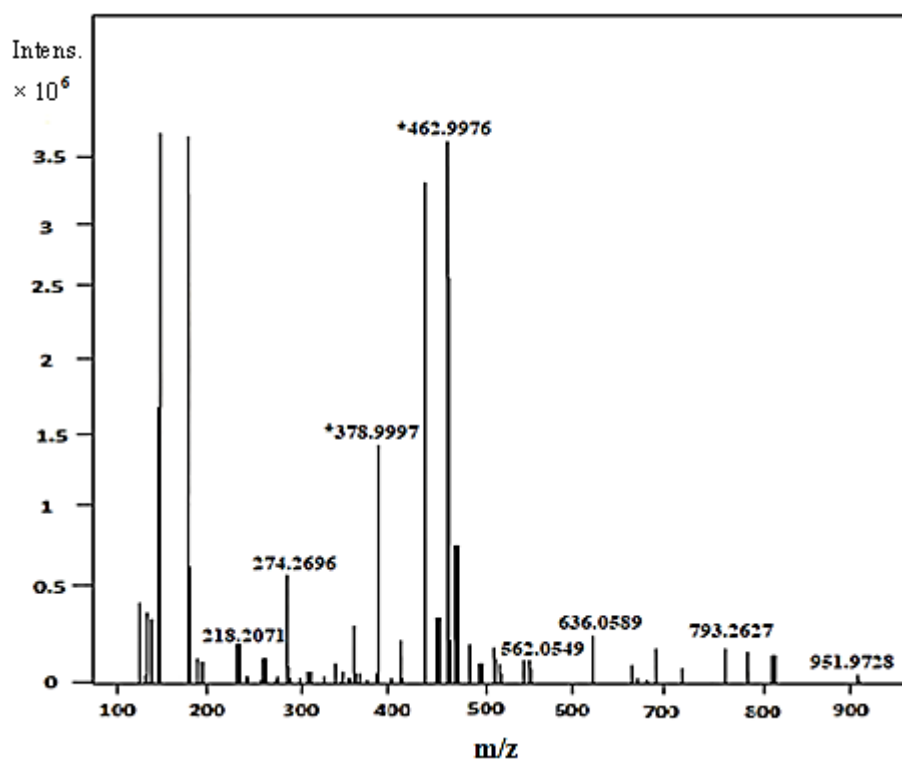
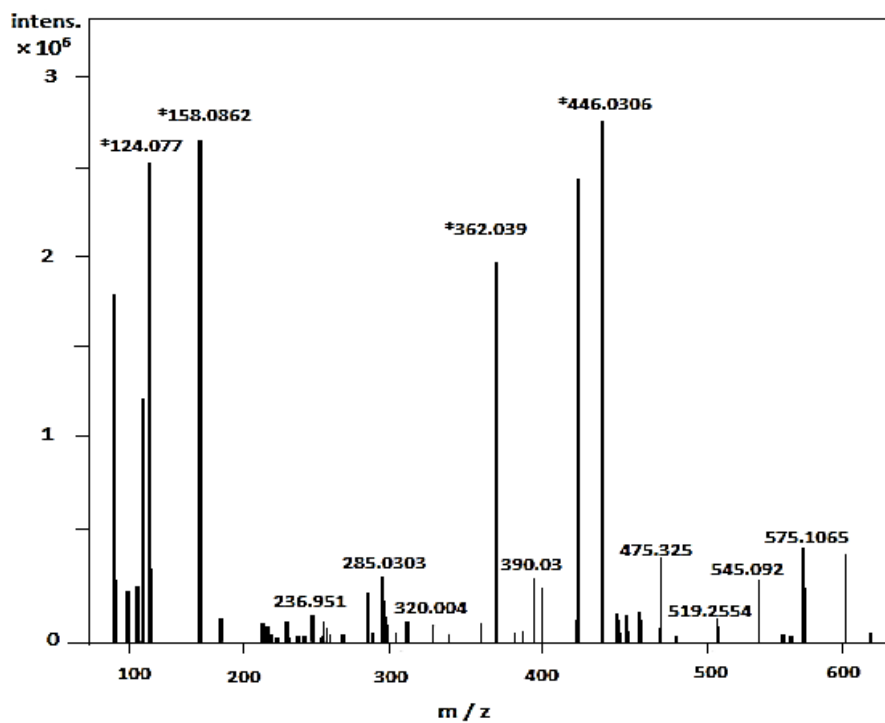**Figure S5.** Mass spectrum in acetonitrile for complex **1**, *m/z*: M⁺ peak at 462.99.

Figure S6. Mass spectrum in acetonitrile for complex **2,** *m/z*: M⁺ peak at 446.03.
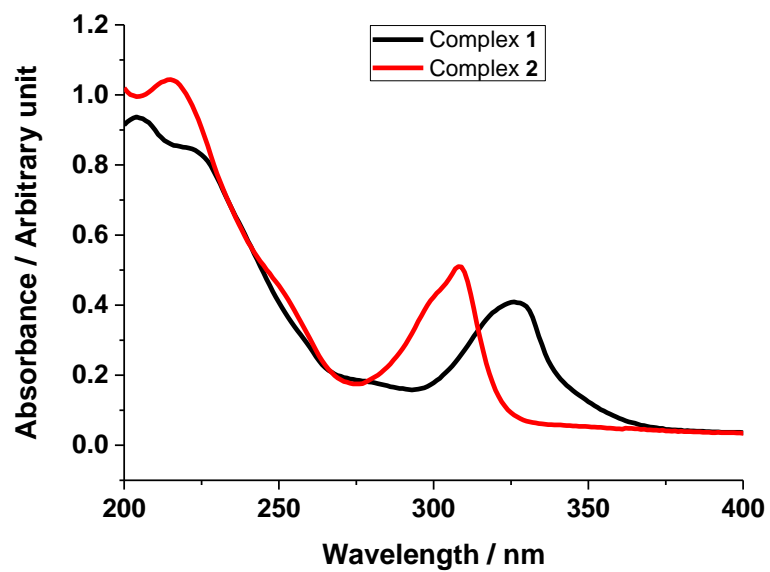
Figure S7.   UV-Vis absorption spectra for complexes **1** (—) and **2** (—) in acetonitrile.

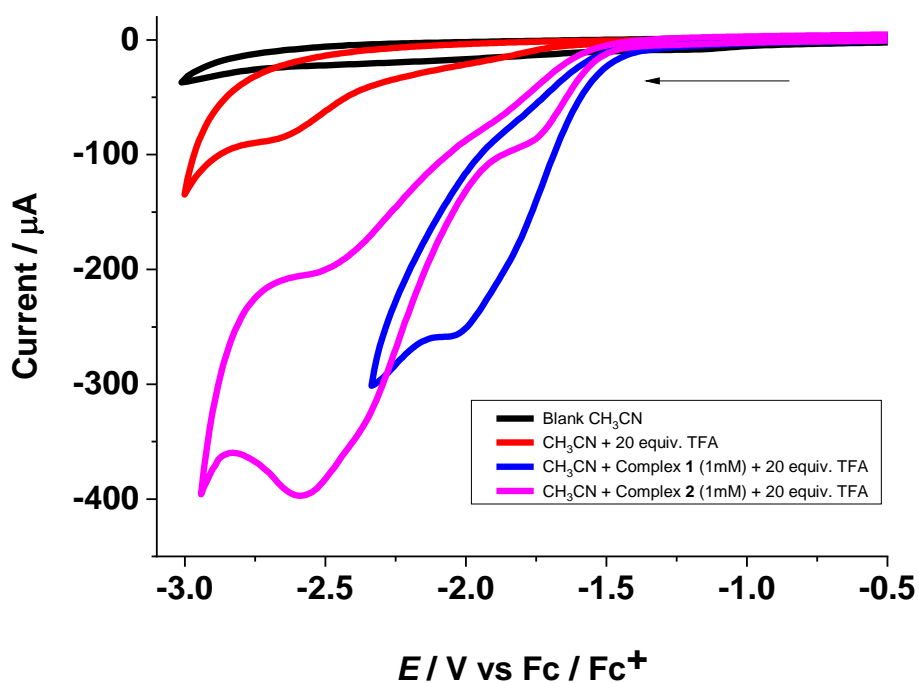**Figure S8.** Cyclic voltammograms (0.1 Vs^{-1}) of CH$_3$CN (—), of CH$_3$CN and 19 mM (20 equiv.) TFA (—), of **1** (1 mM) (—) and of **2** (1 mM) (—) in the presence of 19 mM (20 equiv.) of TFA in CH$_3$CN at 0.1 Vs^{-1}.

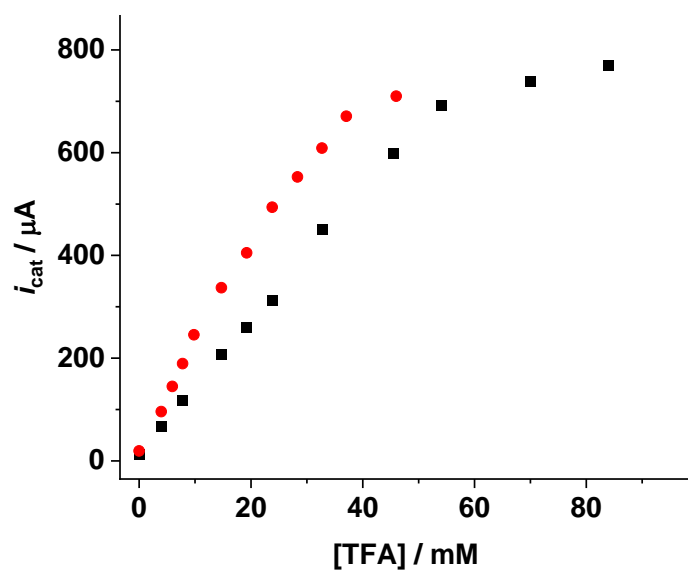**Figure S9.** Plots of i_{cat} *vs.* [TFA]/mM for complexes **1** (■) and **2** (●) in 0.1 M [N(n-Bu$_4$)][PF$_6$] / CH$_3$CN. The negative sign for i_{cat} has been ignored.
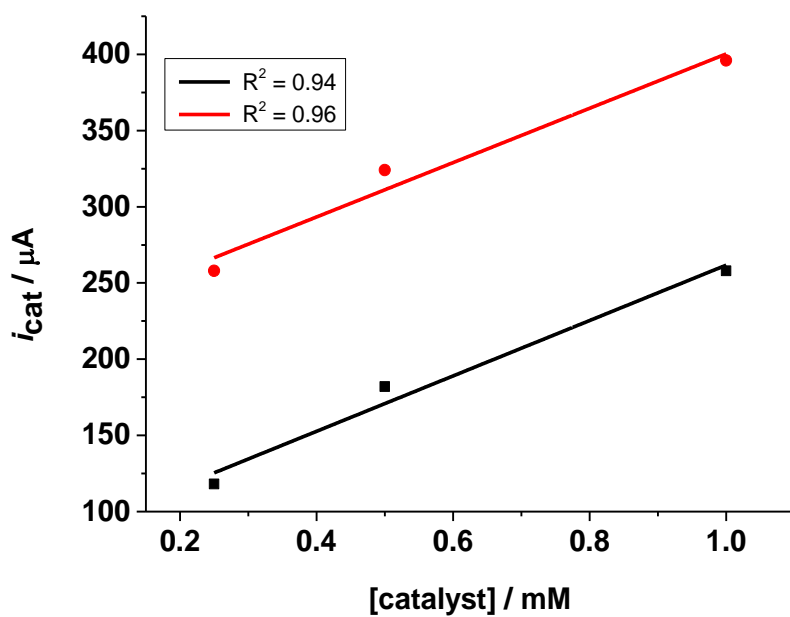
Figure S10. Dependence of i_{cat} on [catalyst] for complexes **1** (■) and **2** (●) in CH_3CN in the presence of 20 equiv. (19 mM) TFA. Lines are best fit lines to the data. The negative sign for i_{cat} has been ignored.
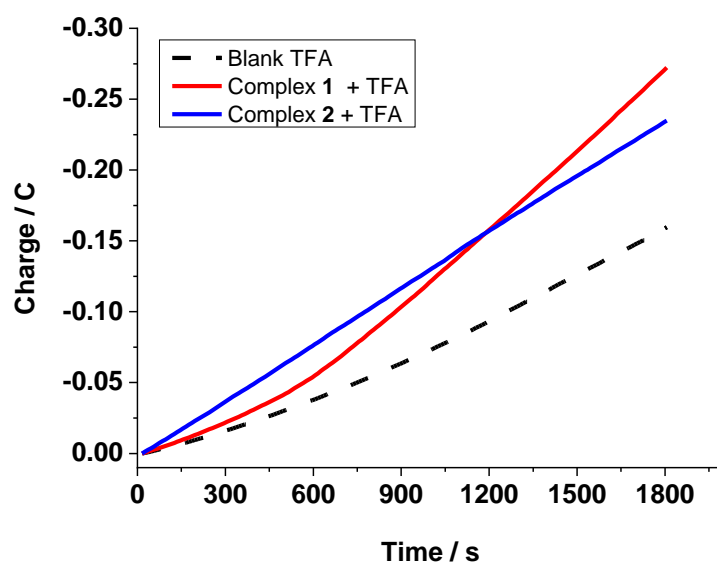
Figure S11. Plots of charge *vs.* time for controlled–potential electrolysis of blank TFA (- - -, 5.95 mM), complexes **1** (—) and **2** (—) (0.25 mM) in CH_3CN / 0.1 M [N(n-Bu$_4$)][PF$_6$] / 5.95 mM (20 equiv.) TFA.

$$TOF = \frac{\Delta C}{F \cdot n_1 \cdot n_2 \cdot t} = \frac{0.1198 \text{ C}}{96480 C \cdot mol^{-1} \times 2 \times 2.5 \times 10^{-6} mol \times 1800} = 1.38 \times 10^{-4} \text{ s}^{-1}$$

Eq. S1. The calculation of *TOF*-complex **1** (TFA).

$$TOF = \frac{\Delta C}{F \cdot n_1 \cdot n_2 \cdot t} = \frac{0.0799 \text{ C}}{96480 C \cdot mol^{-1} \times 2 \times 2.5 \times 10^{-6} mol \times 1800} = 0.92 \times 10^{-4} \text{ s}^{-1}$$

Eq. S2. The calculation of *TOF*- complex **2** (TFA).
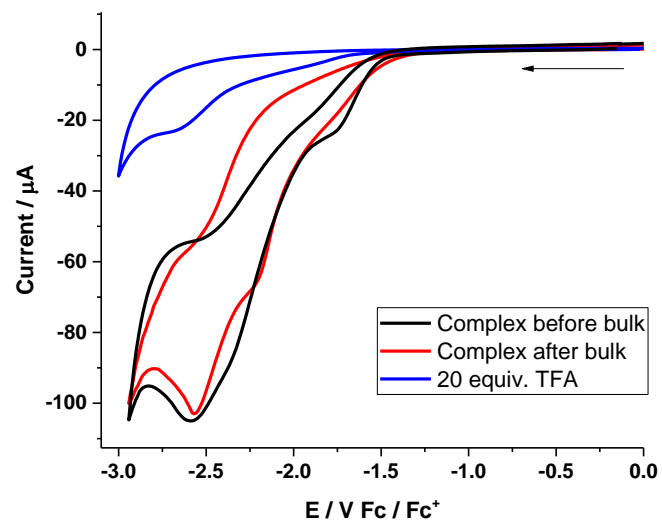
Figure S12. CVs of CH$_3$CN/20 equiv. TFA (—), and complex **2** (0.25 mM) in CH$_3$CN in the presence of 5.95 mM (20 equiv.) TFA before (—) and after (—) 30 min of bulk electrolysis.
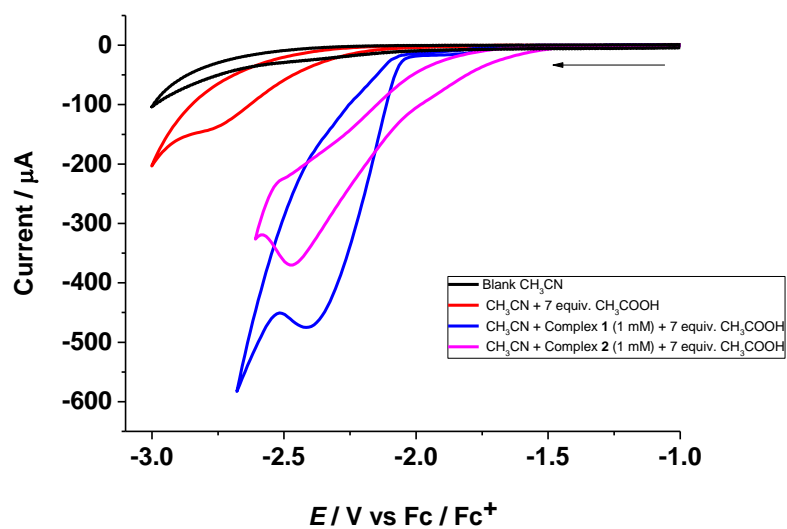
Figure S13. Cyclic voltammograms (0.1 Vs^{-1}) of CH$_3$CN: H$_2$O (1:1) (—), of CH$_3$CN: H$_2$O (1:1) and 7 mM (7 equiv.) CH$_3$COOH (—), of 1 mM **1** (—) and **2** (—) in the presence of 7 mM (7 equiv.) of CH$_3$COOH in CH$_3$CN: H$_2$O (1:1) at 0.1 Vs^{-1}.
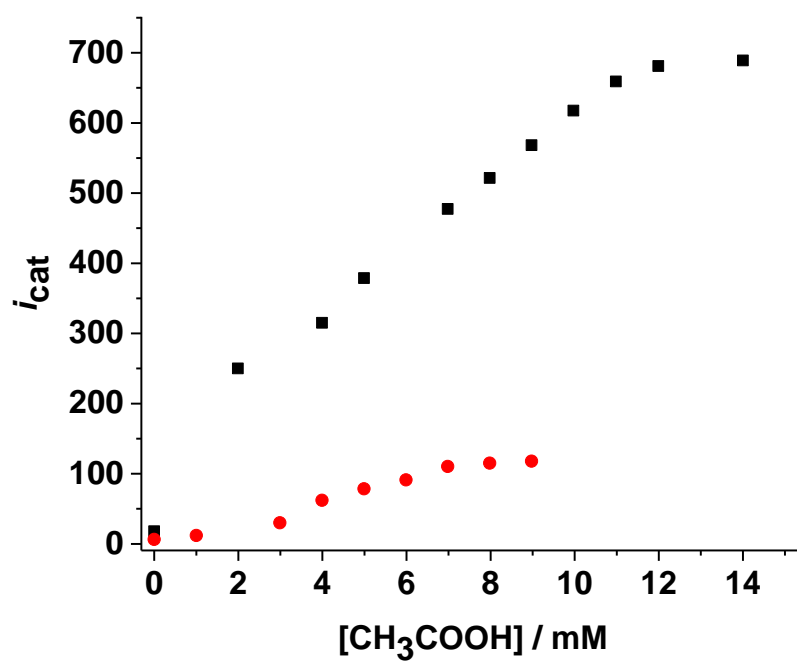
Figure S14. Plots of i_{cat} *vs.* [CH$_3$COOH] / mM for complexes **1** (■) and **2** (●) in 0.1 M [N(n-Bu$_4$)][PF$_6$] / CH$_3$CN: H$_2$O (1:1). The negative sign for i_{cat} has been ignored.

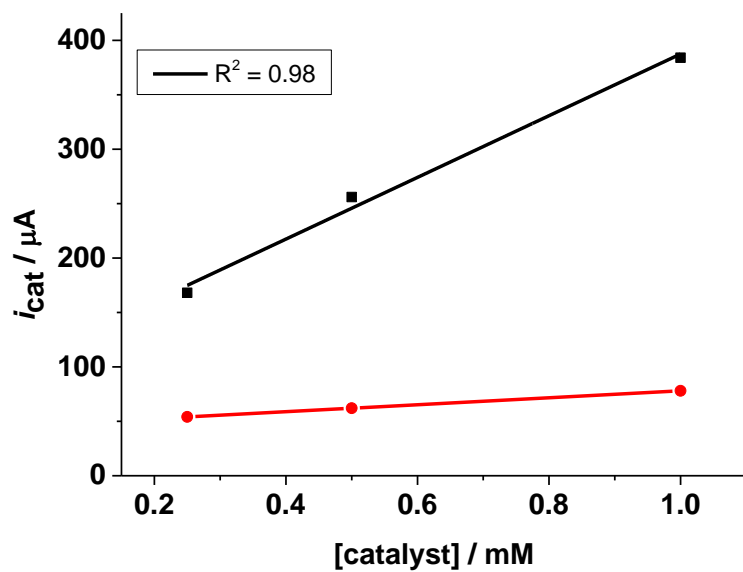**Figure S15.** Dependence of i_{cat} on catalyst concentration for complexes **1** (■) and **2** (●) in 0.1 M [N(n-Bu$_4$)][PF$_6$] / CH$_3$CN:H$_2$O (1:1) in the presence of 7 equiv. (7 mM) CH$_3$COOH. Lines are best fit lines to the data. The negative sign for i_{cat} has been ignored.
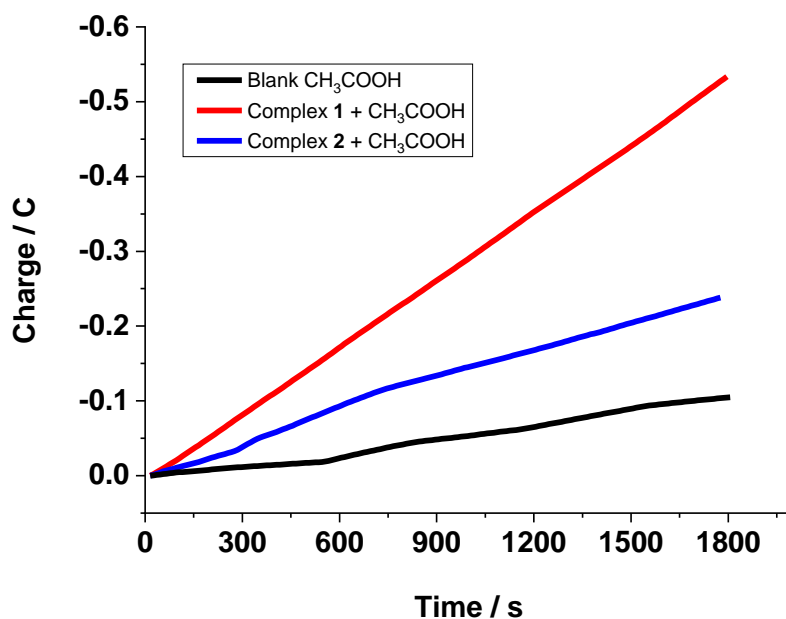
Figure S16. Plots of charge *vs.* time for controlled-potential electrolysis of blank CH₃COOH (—), complexes **1** (—), and **2** (—) (0.25 mM) in CH₃CN : H₂O / 0.1 M [N(n-Bu₄)][PF₆] / 6 mM (6 equiv.) CH₃COOH.

$$TOF = \frac{\Delta C}{F \cdot n_1 \cdot n_2 \cdot t} = \frac{0.4168\ \text{C}}{96480 C \cdot mol^{-1} \times 2 \times 2.5 \times 10^{-6} mol \times 1800} = 4.8 \times 10^{-4}\ \text{s}^{-1}$$

Eq. S3. The calculation of *TOF*-complex **1** (Acetic acid).

$$TOF = \frac{\Delta C}{F \cdot n_1 \cdot n_2 \cdot t} = \frac{0.1337\ \text{C}}{96480 C \cdot mol^{-1} \times 2 \times 2.5 \times 10^{-6} mol \times 1800} = 1.54 \times 10^{-4}\ \text{s}^{-1}$$

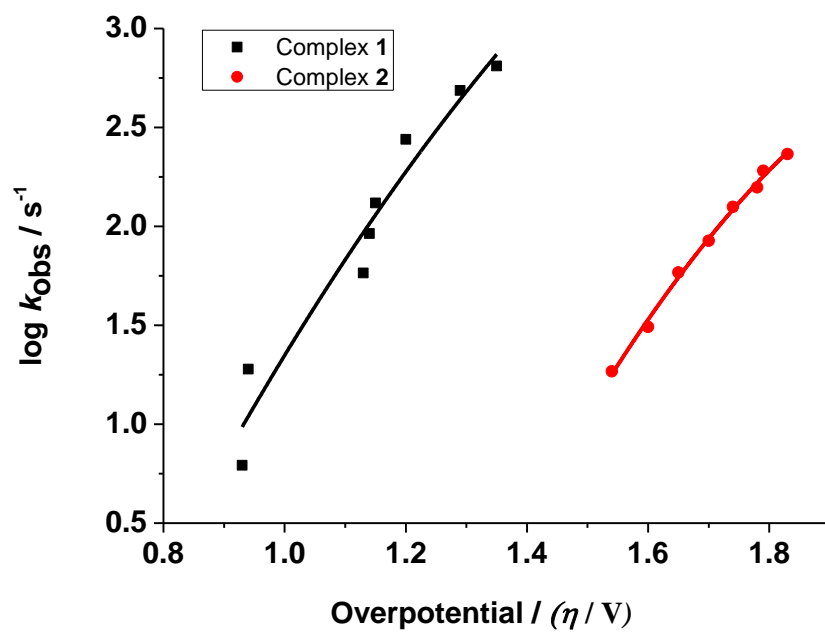**Eq. S4**. The calculation of *TOF*- complex **2** (Acetic acid).

Figure S17. Tafel plots of log k_{obs} *vs.* overpotential for complexes **1** (■) and **2** (●) (CH$_3$CN).

Table S1. Selected bond lengths (Å) and angles (º) for complex **1**.

Bond lengths (Å)		Bond angles (º)	
Mn(1)-P(1)	2.3049(19)	P(1)-Mn(1)-S(1)	88.57(7)
Mn(1)-S(1)	2.444(2)	P(1)-Mn(1)-C(4)	86.56(16)
Mn(1)-N(1)	2.063(6)	S(1)-Mn(1)-C(4)	39.15(16)
Mn(1)-C(4)	2.627(7)	N(1)-Mn(1)-P(1)	85.85(18)
Mn(1)-C(2)	1.867(10)	N(1)-Mn(1)-S(1)	68.78(17)
Mn(1)-C(3)	1.833(7)	N(1)-Mn(1)-C(4)	29.6(2)
Mn(1)-C(10)	1.807(7)	C(2)- Mn(1)-P(1)	90.0(2)
P(1)-C(16)	1.854(6)	C(2)-Mn(1)-S(1)	170.1(2)
P(1)-C(12)	1.838(7)	C(2)-Mn(1)-N(1)	101.3(3)
P(1)-C(11)	1.850(7)	C(2)-Mn(1)-C(4)	130.9(3)
S(2)-C(4)	1.743(7)	C(3)-Mn(1)-P(1)	179.7(2)
S(2)-C(10)	1.758(7)	C(3)-Mn(1)-S(1)	91.1(2)
S(1)-C(4)	1.707(7)	C(3)-Mn(1)-N(1)	94.0(3)
N(1)-C(5)	1.396(9)	C(3)-Mn(1)-C(4)	93.2(3)
N(1)-C(4)	1.317(9)	C(3)-Mn(1)-C(2)	90.3(3)
O(1)-C(1)	1.148(8)	C(1)-Mn(1)-P(1)	90.4(2)
O(3)-C(3)	1.143(9)	C(1)-Mn(1)-S(1)	95.9(2)
O(2)-C(2)	0.980(9)	C(1)-Mn(1)-N(1)	164.3(2)
		C(1)-Mn(1)-C(4)	135.0(3)
		C(1)-Mn(1)-C(2)	93.9(3)
		C(1)-Mn(1)-C(3)	89.7(3)

Table S2.   FTIR data for complexes **A**, **B**, **1** and **2** in dichloromethane.

Complexes	Wavenumber / cm^{-1}
[$Mn_2(CO)_6(\mu\text{-}S_2NC_7H_4)_2$] **A**	2036, 2012, 1919
[$Mn_2(CO)_6(\mu\text{-}SN_2C_7H_5)_2$] **B**	2032, 2015, 1963, 1920
fac-[$Mn(CO)_3(\kappa^2\text{-}S_2NC_7H_4)(PTA)$] **1**	2022, 1941, 1902
fac-[$Mn(CO)_3(\kappa^2\text{-}SN_2C_7H_5)(PTA)$] **2**	2021, 1940, 1903

Table S3.   UV-Vis data for complexes **1** and **2** in acetonitrile.

Complexes	Wavelength / nm
fac-[$Mn(CO)_3(\kappa^2\text{-}S_2NC_7H_4)(PTA)$] **1**	326, 222(sh), 204(sh)
fac-[$Mn(CO)_3(\kappa^2\text{-}SN_2C_7H_5)(PTA)$] **2**	308, 214(sh)